# Effect of Joule heating on isoelectric focusing of proteins in a microchannel

Kisoo Yoo,[1,a)] Jaesool Shim,[2,a)] and Prashanta Dutta[1,b)]
[1]*School of Mechanical and Materials Engineering, Washington State University, Pullman, Washington 99164-2920, USA*
[2]*School of Mechanical Engineering, Yeungnam University, Gyeongsan, Gyeonsanbukdo, South Korea*

(Received 5 September 2014; accepted 9 December 2014; published online 18 December 2014)

Electric field-driven separation and purification techniques, such as isoelectric focusing (IEF) and isotachophoresis, generate heat in the system that can affect the performance of the separation process. In this study, a new mathematical model is presented for IEF that considers the temperature rise due to Joule heating. We used the model to study focusing phenomena and separation performance in a microchannel. A finite volume-based numerical technique is developed to study temperature-dependent IEF. Numerical simulation for narrow range IEF ($6 < \text{pH} < 10$) is performed in a straight microchannel for 100 ampholytes and two model proteins: staphylococcal nuclease and pancreatic ribonuclease. Separation results of the two proteins are obtained with and without considering the temperature rise due to Joule heating in the system for a nominal electric field of 100 V/cm. For the no Joule heating case, constant properties are used, while for the Joule heating case, temperature-dependent titration curves and thermo-physical properties are used. Our numerical results show that the temperature change due to Joule heating has a significant impact on the final focusing points of proteins, which can lower the separation performance considerably. In the absence of advection and any active cooling mechanism, the temperature increase is the highest at the midsection of a microchannel. We also found that the maximum temperature in the system is a strong function of the $\Delta$pK value of the carrier ampholytes. Simulation results are also obtained for different values of applied electric fields in order to find the optimum working range considering the simulation time and buffer temperature. Moreover, the model is extended to study IEF in a straight microchip where pH is formed by supplying $H^+$ and $OH^-$, and the thermal analysis shows that the heat generation is negligible in ion supplied IEF. © *2014 AIP Publishing LLC*.
[http://dx.doi.org/10.1063/1.4904805]

## I. INTRODUCTION

Electric field-driven separation techniques are widely used in the purification of ions, proteins, and DNA. Among various electro-separation processes, isoelectric focusing (IEF) is very popular for the separation of proteins because it offers very high resolution, even for proteins or charge components with close isoelectric points (pH points of zero net charge). In addition, IEF is capable of increasing the concentration of components by two to three orders of magnitude from its initial concentration.[1] Because of these favorable attributes, IEF has become the ubiquitous technique in modern proteomics. As with any other electro-separation technique, IEF is initiated by applying an electric field through an external electric potential difference.

[a)]K. Yoo and J. Shim contributed equally to this work.
[b)]Author to whom correspondence should be addressed. Electronic mail: prashanta@wsu.edu.

 

In the last three decades, IEF has been studied extensively, both experimentally[2–4] and theoretically.[5] The theoretical study of IEF is very challenging due to the large number of mass conservation equations needed to describe how ampholytes form a smooth pH profile in the system. For this reason, most of the early attempts to study IEF were limited to several dozen ampholytes and/or one-dimensional (1-D) geometry, and the resultant pH profiles were stair-step in shape. Recently, due to the availability of high performance computers and the development of efficient parallel algorithms, it is possible to simulate several hundred ampholytes in order to form smooth profiles for both narrow- and broad-range IEF.[6,7] Although the aforementioned IEF simulations have been used to explain experimental behavior in 1-D[8,9] and two-dimensional (2-D)[10–12] problems qualitatively, none of these models have accounted for the effect of temperature. All previous IEF models were based on the same reference temperature, with no consideration of Joule heating in the capillary tube or microchannels. However, Joule heating is an essential component of any electrolyte-based electro-separation technique.[13] The interaction between the applied electric field and the charged ions causes heat generation in the system.[14,15] Unlike a linear electro-separation technique, this heat generation is not uniform along the channel for IEF due to the nonuniform local electric field and ionic conductivity. Thus, we must understand the contribution of Joule heating and it effects for an evaluation of separation performance. For instance, Joule heating might cause localized drying of electrolytes or peak broadening. These adverse effects are even more serious if the separation channel is made out of insulating materials, or if there is no external cooling mechanism.

A few studies have been reported in the literatures that describe the role of Joule heating in electrokinetic separation. In 1989, Grushka *et al.*[16] studied the effect of temperature gradients on the efficiency of capillary electrophoresis separations. They reported that Joule heating leads to a temperature-dependent flow velocity, which causes a loss in separation efficiency at high temperature. Ghosal[17] reviewed band dispersion due to Joule heating in capillary electrophoresis where the operating voltage is on the order of kilovolts. Recently, Shim and Dutta[18] developed a model for constant voltage mode isotachophoresis. However, none of the aforementioned models considered the effect of Joule heating in microchip IEF. Theoretical study of ampholyte based IEF is much more challenging than any other electrokinetic phenomena as one has to solve hundreds of partial differential equations for ampholytes to form smooth pH profile. The core focus of this study is to understand the effect of Joule heating in ampholyte based microchip IEF. We specifically studied the effect of Joule heating on the transient focusing behavior of staphylococcal nuclease and pancreatic ribonuclease in a pH field under the action of an applied electric field. The focusing positions of the two model proteins are compared with and without considering Joule heating. The discrepancies in the focusing positions are explained with respect to the local temperature and heat generation in the system. The effect of the applied electric field is also studied to determine the end of the separation time and the maximum temperature in the channel. Furthermore, the maximum temperatures along the channel are studied by varying the dissociation constants of the ampholytes. Finally, we studied the thermal characteristics in the newly introduced microchip IEF,[4,19] where pH is formed by supplying hydrogen and hydroxyl ions to show the contrasts with ampholyte based IEF.

## II. MATHEMATICAL MODEL OF ISOELECTRIC FOCUSING

### A. Governing equations

Isoelectric focusing is a special type of field gradient electrofocusing technique in which analytes such as proteins or enzymes are separated at their isoelectric points (p*I*s) in the presence of a pH field. Generally, carrier ampholytes (low molecular weight amphoteric molecules) are used to form a pH gradient in the system. The carrier ampholytes are loaded into the separation device at the time of introducing the analytes. Figure 1 shows a schematic of IEF separation of two sample proteins in a straight microchannel.

In microchip or capillary IEF, a nonuniform temperature rise takes place due to heat generation from Joule heating. This nonuniform heating can adversely affect the separation

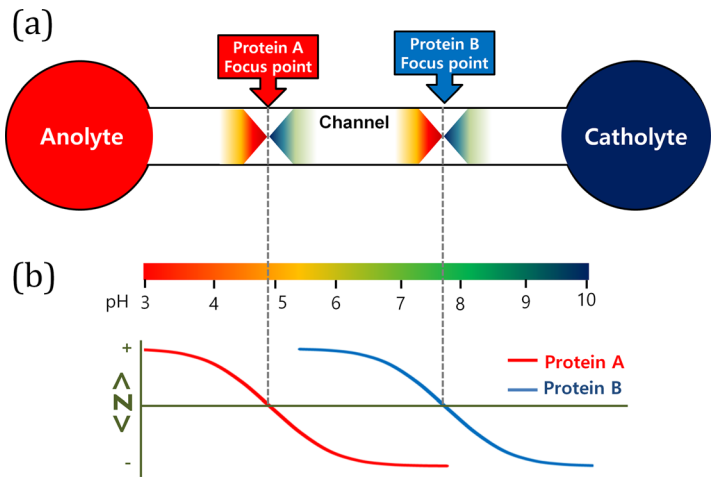


FIG. 1. (a) Schematic diagram of a 2-D planar channel used to simulate the isoelectric focusing of two proteins. The anode and cathode are placed at the left (anolyte) and right (catholyte) reservoirs, respectively. This figure is not to scale. (b) Titration curves for two proteins. Under the action of an applied electric field, proteins will be focused at their isoelectric points (p*I*s), pH of zero net charge. A protein will be positively charged at a pH value lower than its p*I* value, and will be negatively charged at a pH higher than its p*I* value.

performance, especially if there is no active heat removal mechanism. In traditional ampholyte based IEF, bulk fluid motion due to electroosmosis is suppressed to improve the efficiency of the separation. Thus, the contribution of advection is negligible, and the transient temperature distribution along a microchannel (Fig. 1) can be expressed using the following energy equation:[20]

$$\rho C_p \left(\frac{\partial T}{\partial t}\right) = \nabla \cdot (k \nabla T) + S, \tag{1}$$

where $T$ is the temperature, and $\rho$, $k$, and $C_p$ are the mass density, thermal conductivity, and specific heat of the buffer solution, respectively, in the IEF system. The source term in Eq. (1) can be approximated as $S = \sigma (\vec{E} \cdot \vec{E})$ (see Appendix A for more details), where $\vec{E}$ is the local electric field due to the electric potential ($\phi$) gradient in the system. The ionic conductivity $\sigma$ of the buffer solution can be obtained from the concentration of individual components in the system as follows:

$$\sigma = F\left[\sum_{i=1}^{M} (\langle z_i^2 \rangle \omega_i C_i)\right], \tag{2}$$

where $C_i$ and $\omega_i$ are the concentration and absolute mobility of each component including hydrogen ($H$) and hydronium ($OH$) ions, $M$ is the total number of components, and $\langle z_i^2 \rangle$ is the effective mean square valence of each amphoteric component. Here, all thermo-physical properties such as density, thermal conductivity, and specific heat, and electrochemical properties such as ionic conductivity and absolute mobility, are functions of temperature.

In an IEF system, the concentration of the $i$ th amphoteric component can be found by summing concentration ($S_{ij}$) of all $J_i + 1$ species of component $i$ in the system with a total of $J_i$ dissociable groups, as follows:[11]

$$C_i = \sum_{j=1}^{J_i+1} S_{ij}. \tag{3}$$

Therefore, for an infinitely dilute solution, the mass conservation equation of each component is given as

$$\frac{\partial C_i}{\partial t} - \nabla \cdot [\omega_i \langle z_i \rangle \nabla \phi \, C_i + D_i \nabla C_i] = 0, \tag{4}$$

where $\langle z_i \rangle$ and $D_i$ are the net charge and diffusion coefficient of each component $i$, respectively. The diffusion coefficient is related to the absolute mobility by the Nernst-Einstein equation,[21]

$$D_i = \frac{RT\omega_i}{F},$$

where $F$ is the Faraday constant and $R$ is the universal gas constant. The net charge $\langle z_i \rangle$ of component $i$ can be calculated from species charges ($z_{ij}$) as

$$\langle z_i \rangle = \frac{\sum_{j=1}^{J_i+1} z_{ij} S_{ij}}{C_i}. \tag{5}$$

The mass conservation equation (4) is also known as the Nernst-Planck equation. The electric field ($\vec{E} = -\nabla\phi$) in the mass conservation equation can be calculated from the following charge conservation equation:

$$\nabla \cdot \left( F \left[ \sum_{i=1}^{M-2} \left( \langle z_i^2 \rangle \omega_i C_i \right) + \omega_H C_H + \omega_{OH} \frac{K_w}{C_H} \right] \nabla \phi \right.$$
$$\left. + F \left[ \sum_{i=1}^{M-2} (D_i \langle z_i \rangle \nabla C_i) + D_H \nabla C_H - D_{OH} \nabla \left( \frac{K_w}{C_H} \right) \right] \right) = 0, \tag{6}$$

where $K_W$ is the dissociation constant of water. The effective mean square valance ($\langle z_i^2 \rangle$) of each component can be defined as[22]

$$\langle z_i^2 \rangle = \frac{\sum_{j=1}^{J_i+1} z_{ij}^2 S_{ij}}{C_i}. \tag{7}$$

In an IEF system, the concentrations of hydrogen and hydroxyl ions are very important for the calculation of the pH profile in the channel, and for the solution of the charge and energy conservation equations. The component mass conservation equation (Eq. (4)) can be used for the computation of hydrogen and hydroxyl ions. While mathematically accurate and acceptable, a determination of the hydrogen ion concentration using the Nernst-Planck equation is very challenging as the hydrogen ion concentration changes by several orders of magnitude along the channel. Thus, to circumvent the numerical challenges, the concentration of hydrogen ions can be calculated from the following electroneutrality condition:

$$C_H - \frac{K_W}{C_H} + \sum_{i=1}^{M-2} (\langle z_i \rangle C_i) = 0. \tag{8}$$

We note that the electroneutrality condition is not valid close to the wall where the electric double layer might form. Thus, for nanochannel IEF, the Poisson-Nernst-Planck model[23–25] must be solved. However, in this study, the length scale of the electric double layer is three to four orders of magnitude smaller than the length scale of a typical microfluidic device used for IEF.

Thus, a complete mathematical description for temperature-dependent IEF consists of Eq. (1) for temperature; Eqs. (4) and (8) for the concentration of amphoteric components and hydrogen ions; and Eq. (6) for electric potential. It is noteworthy to mention that the contribution of the advection term is not considered in the mass, charge, and energy conservation equations. This is because bulk motion of the buffer is undesirable in IEF—the bulk fluid flow disperses the focused bands and reduces the separation resolution and efficiency. Nevertheless, the applied electric field might create electroosmotic flow in the separation channel. For that reason, the IEF channel is typically coated with chemicals to suppress undesired electroosmotic flow.[1,3] The effects of electroosmosis are studied extensively for capillary zone electrophoresis[17,26,27] and isoelectric focusing.[28] In this study, we assume that our channels are perfectly coated to knock down the electroosmosis so that the detrimental effects of Joule heating can be studied precisely.

All governing equations are coupled in temperature-dependent IEF. For example, concentrations of amphoteric components are needed for the computation of ionic conductivity in the energy conservation equation. Similarly, for the solution of mass conservation equations, we must know properties such as absolute mobilities, diffusivities, and net charges, which strongly depend on temperature. Moreover, using the charge conservation equation, the electric potential must be determined for the mass and energy conservation equations; electroneutrality equation must be solved in order to obtain the local pH value needed for the net charge of amphoteric components in the mass conservation equations.

### B. Boundary conditions

In this study, temperature-dependent IEF is simulated in a 2-D straight microchannel, as shown in Fig. 1, where an external electric field is applied between the anolyte (left) and catholyte (right) reservoirs. Thus, the computational domain is limited to the channel region only. For the mass conservation equation, a zero net flux is implemented at the junctions of the reservoirs and channel; there is no penetration at the channel surface. The charge conservation equation is subjected to electrically insulating boundary conditions at the channel surface, and a known applied potential at the junctions of the channel and reservoirs. Similarly, for the energy conservation equations, thermally insulating boundary conditions are specified at the channel surface, and known temperatures are specified at the reservoir and channel junctions. Both the thermally and electrically insulating boundary conditions are well justified at the channel surface because glass, poly di-methyl siloxane (PDMS), or other insulating materials are generally used for microchannel walls.

## III. TEMPERATURE-DEPENDENT PROPERTIES

In temperature-dependent IEF, all governing equations are fully coupled through properties such as density $(\rho)$, isobaric specific heat $(C_p)$, thermal conductivity $(k)$, ionic conductivity $(\sigma)$, diffusion coefficient $(D_i)$, and absolute mobility $(\omega_i)$. Since these properties are strong functions of temperature, it is imperative to use temperature-dependent properties to study the effect of Joule heating on IEF separation performance. Table I summarizes the temperature-dependent properties used in this study. For thermo-physical properties such as density, specific heat, and

TABLE I. Thermo-physical properties for temperature-dependent isoelectric focusing. Here, $T_\infty$ is the reference temperature, which is set as 20 °C.

| Properties | Symbol | Temperature correction equation | Unit |
|---|---|---|---|
| Density | $\rho$ | $999.62 - 0.3759(T - T_\infty)$ | kg/m$^3$ |
| Heat capacity | $C_p$ | $4186.7 - 0.8651(T - T_\infty) + 0.0177(T - T_\infty)^2$ | kJ/kg K |
| Thermal conductivity | $k$ | $k_o(1 + 0.02(T - T_\infty))$; $k_o = 0.61$ (W/m K) | W/m K |
| Absolute mobility | $\omega_i$ | $\omega_o(1 + 0.02(T - T_\infty))$; $\omega_o = 3\text{E-}8$ (m$^2$/V s) | m$^2$/V s |
| Diffusion coefficient | $D_i$ | $\frac{8.13T\omega_i}{96485}$ | m$^2$/s |

thermal conductivity, the temperature-dependent properties of water are used due to the very dilute buffer solution. The density of water linearly decreases with increasing temperature in the IEF operation range (between 20 and 90 °C), and thus a linear temperature correction is used for density. On the other hand, the heat capacity changes nonlinearly in the IEF operation range. For this reason, the temperature correction for heat capacity at constant pressure is formulated as a second-order polynomial equation. The thermal conductivity ($k$) and absolute mobility ($\omega_i$) are expressed as a linear function of temperature as described in Refs. 29 and 30. The temperature-dependent diffusion coefficient ($D_i$) is calculated using the Nernst-Einstein equation.[21]

The effective valance ($\langle z_i \rangle$) of carrier ampholytes is assumed to be independent of temperature and to be only dependent on pH. This is because carrier ampholytes have an active charge distribution in a very narrow range. Moreover, carrier ampholytes can be engineered to satisfy this and many other constraints because they are synthesized artificially to create a favorable pH platform for IEF. However, for most proteins, the effective valance is strongly dependent on temperature.[31,32] In this study, staphylococcal nuclease and pancreatic ribonuclease are selected as model proteins for temperature-dependent IEF simulation. The titration curves of these two proteins (Fig. 2) are obtained from the experimental work of Dick *et al.*[32] for two different temperatures: 25 and 100 °C. We have developed eleventh-order polynomial equations to precisely represent the titration curves shown in Fig. 2. Next, we have used a linear interpolation scheme to form temperature-dependent titration curves for model proteins as

$$z(T) = \frac{\text{T–100}}{\text{25–100}}\text{z}(25\,^{\circ}\text{C}) + \frac{\text{T–25}}{\text{100–25}}\text{z}(100\,^{\circ}\text{C}). \tag{9}$$

Equation (9) is used to find the temperature-dependent effective valance ($\langle z_i \rangle$) for any temperature between 20 °C (the reference temperature) and 100 °C. Also, the effective mean square valance ($\langle z_i^2(pH,T) \rangle$) is obtained from the titration curve as follows:[7]

$$\langle z_i^2(pH,T) \rangle = [f_i(pH,T)]^2 - \frac{1}{\ln(10)} \frac{df_i(pH,T)}{dpH}, \tag{10}$$

where $f_i(pH,T) = \langle z_i(pH,T) \rangle$.

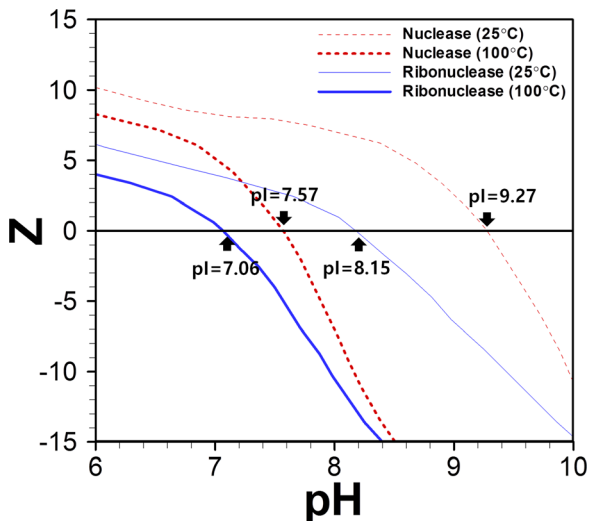


FIG. 2. Temperature-dependent titration curves for two model proteins (staphylococcal nuclease and pancreatic ribonuclease).

## IV. NUMERICAL METHODS

Discretized algebraic equations are obtained for the unsteady mass and energy conservation equations, and the steady charge conservation equation, using a finite volume approach.[33] The unsteady term in the Nernst-Planck equations and the energy equation is modeled with a first order-accurate implicit scheme. The power law scheme is used to compute the net flux terms in the mass, charge, and energy conservation equations. In the absence of any advection term, the electro-migration term is used to calculate the flow strength. In other words, in the exponential scheme, the cell Peclet number is calculated as the ratio of diffusion strength to electro-migration strength. The Newton-Raphson method is employed to find the concentration of hydrogen ions from the electro-neutrality equation. Since all the governing equations are coupled, an iterative solution technique is used in this study.

Figure 3 shows the algorithm used in this study for temperature-dependent IEF. First, all variables such as temperature, the concentration of ampholytes, the concentration of proteins, the concentration of hydrogen, and the electric potential are initialized throughout the computational domain with a uniform value. Next, the energy conservation equation is solved to obtain a temperature distribution along the channel due to Ohmic/Joule heating from the applied electric field. The temperature value obtained from the energy conservation equation is used to correct properties such as density, specific heat, thermal conductivity, absolute mobility, the diffusion coefficient, and net charge. Next, the mass and charge conservation equations are solved

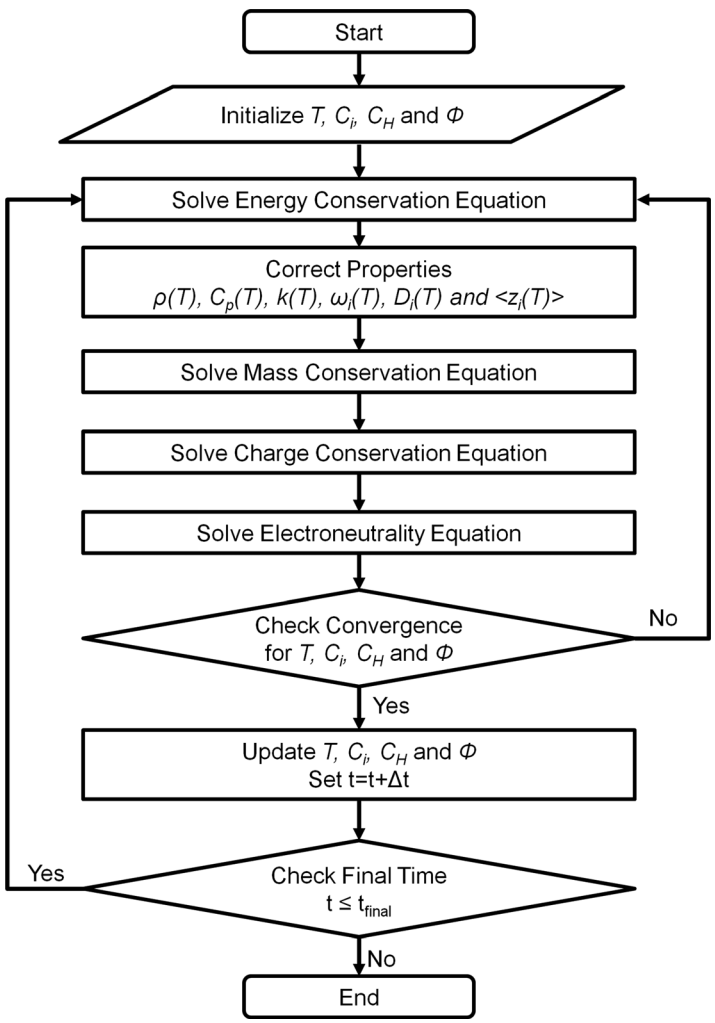


FIG. 3. Flow chart of temperature-dependent IEF simulation for protein separation.

followed by the electroneutrality equation. Since an iterative scheme is used, convergences are checked after each iteration process. For the mass, energy, and charge conservation equations, a convergence tolerance of $10^{-5}$ is used. A convergence tolerance of $10^{-4}$ is used for the electroneutrality equation. All pertinent variables are updated once all of the variables converged within the tolerance limit. The solution procedure is continued until the final time is reached.

## V. RESULTS AND DISCUSSION

Temperature-dependent IEF simulations are conducted in a 2-D straight microchannel (2 cm × 100 $\mu$m × 10 $\mu$m) as shown in Fig. 1. Unless stated otherwise, all simulation results are obtained for ampholyte based IEF. A narrow pH range between 6 and 10 is selected since the pI points of the target proteins are located between 6.5 and 9.5. The pH profile is formed with the aid of 100 ampholytes to set the stage for isoelectric focusing of proteins. In this study, ampholytes are considered as biprotic; i.e., only two dissociation constants near their isoelectric points have a significant effect on the transient behavior of the carrier ampholytes. For simplicity, the isoelectric points of the ampholytes are uniformly spanned between the anode and cathode with a $\Delta pI = 0.04$. Ribonuclease and nuclease are used as model protein for IEF separations in microchannel. At the reference temperature of 20 °C, the isoelectric points of ribonuclease and nuclease are 8.315 and 9.385, respectively. The reference absolute mobility $(\omega_0)$ of proteins and ampholytes is fixed at 3.0E-8 $m^2/V{\cdot}s$. For the ampholytes, temperature correction is only applied to the absolute mobility term. For proteins, temperature correction is applied to both the absolute mobility and net charge. As previously mentioned, the electric field-induced electroosmotic flow is not considered since most of the IEF column/channel is coated with chemicals to suppress the electroosmotic flow. It is assumed that the ionic strengths do not affect the electrophoretic mobilities of ampholytes and proteins, as reported in Ref. 10. The initial concentrations of ampholytes and proteins are set as 0.2 mM and 2 $\mu$M, respectively, throughout the separation column.

### A. Constant temperature IEF

The transient profiles of amphoteric components such as ampholytes and proteins are shown in Fig. 4 for a constant temperature IEF at a nominal electric field of 100 V/cm. In this case, the base (reference) temperature is set to 20 °C, and it is assumed that the temperature does not change with time. As shown in Fig. 4(a), ampholytes having isoelectric points (p*I*s) close to the electrode reservoirs focus first, and the focusing process progresses toward the

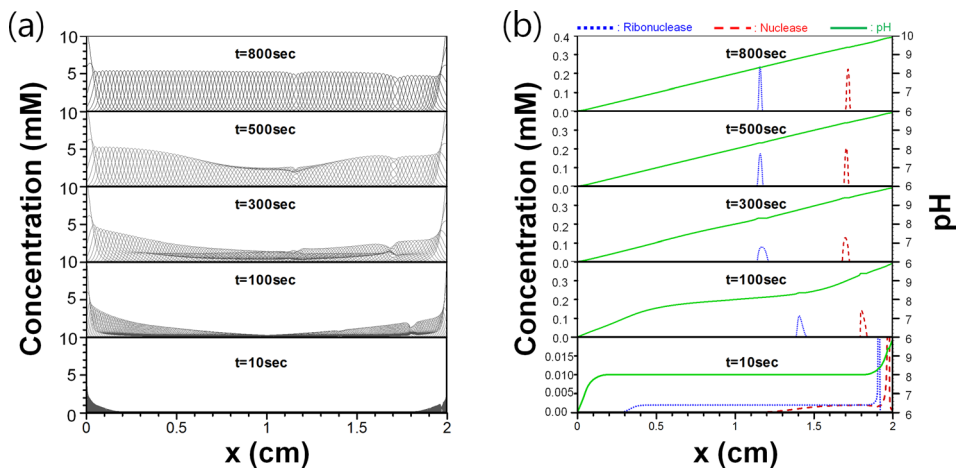


FIG. 4. Concentration distribution of (a) ampholytes and (b) proteins along a straight microchannel without considering Joule heating effect in microchip IEF. Numerical results are extracted at the channel centerline (along the center line in Fig. 1). The potentials at the anodic side and cathodic side are 200 and 0 V, respectively. One hundred biprotic ampholytes ($\Delta pK = 3.0$) are used to form a pH range between 6 and 10.

center of the channel over time. The ampholyte focusing process is completed within 800 s, and Gaussian concentration profiles with uniform peak widths are obtained for most ampholytes (with a few exceptions). The peak height of ampholytes that focused close to the electrode reservoirs is higher than the regular peak height (~5.1 mM) because the slopes of the titration curves are much steeper for ampholytes close to the electrode reservoirs compared to others. On the other hand, the peak heights of some other ampholytes are lower than the regular heights due to the fact that their focused points are very close to the proteins.

Figure 4(b) shows that the focus point and peak concentration of a protein changes with time until the end of the separation stage. The focus positions of proteins change as the pH profiles develop with time. Initially, the pH profile is very flat except at a location very close to the wall. As time progresses, a linear-like pH profile is formed, and the pH profile is almost developed at 500 s as shown in Fig. 4(b). Afterwards, the change in the pH profile is not noticeable (except at the protein locale), and the focused positions of proteins also do not change appreciably after 500 s. However, there is a significant change in the bandwidth and peak heights of proteins between 500 and 800 s. During the final stage of separation, the protein concentration increases due to the sharpening of the pH profiles at the protein locale. At 800 s, the concentration of ribonuclease is slightly higher than the nuclease, while at 500 s and earlier, the concentration of nuclease is higher than that of ribonuclease. The change of protein concentrations during the final stage of separation is primarily affected by the pH gradient (dpH/dx) and net charge gradient (dz/dpH). It is important to note that in constant temperature IEF, the net charge gradient at the p*I* point remains the same for a particular protein. As shown in Fig. 2, at the pI points, the titration curve is much steeper (higher net charge gradient) for nuclease ($dz/dpH = -12.631$) compared to ribonuclease ($dz/dpH = -6.715$). Thus, in a linear pH profile or uniform pH gradient, the concentration of nuclease should be higher than that of ribonuclease. Ideally, the nominal value of the pH gradient should be $2\,cm^{-1}$ throughout the channel during the final stage of separation. However, our numerical results predict that the local pH gradient is significantly lower for nuclease ($0.3781\,cm^{-1}$) and ribonuclease ($0.3876\,cm^{-1}$) at $t = 500$ s because of the high charge values of the proteins and the limited number of ampholytes. The ideal pH gradient can be achieved if the number of ampholytes can be increased by 10 to 20 fold. Nevertheless, since the local pH gradient is quite comparable for both proteins, the concentration of nuclease is higher than ribonuclease at $t = 500$ s.

At $t = 800$ s, the local pH gradient improves significantly for ribonuclease ($0.8621\,cm^{-1}$), while it increases moderately for nuclease ($0.45847\,cm^{-1}$). Consequently, the concentration of ribonuclease is higher than that of nuclease at $t = 800$ s. There is no change in the concentration of ampholytes and proteins after 800 s, and we call this the end of the separation phase. At the end of the separation phase, the concentrations of ribonuclease and nuclease reach 0.24 and 0.22 mM, respectively. Thus, the IEF process is able to achieve 100-fold increases in concentration as well as base line separation between two proteins, which is a signature characteristic of ampholyte based IEF.

### B. Temperature-dependent IEF

Figure 5 shows the transient concentration distribution of proteins and ampholytes for temperature-dependent IEF simulation. Unlike the results presented in Fig. 4, the contribution of temperature is taken into consideration to find the transient behavior of ampholytic components. In an electric field-driven IEF process, the temperature changes in the channel as a result of the generation of heat from the interaction of the electrolyte and ionic current, as discussed in Sec. V C. In temperature-dependent IEF, two major differences can be observed from the no Joule heating case presented in Fig. 4.

First, the focusing speed of ampholytes is much faster than that of the no Joule heating case. This is because the mobility of ampholytes increases with temperature. Numerical results reveal that the protein concentration profiles become fully developed at 500 s, whereas it takes more than 700 s to reach a fully developed profile in the case of constant temperature IEF.

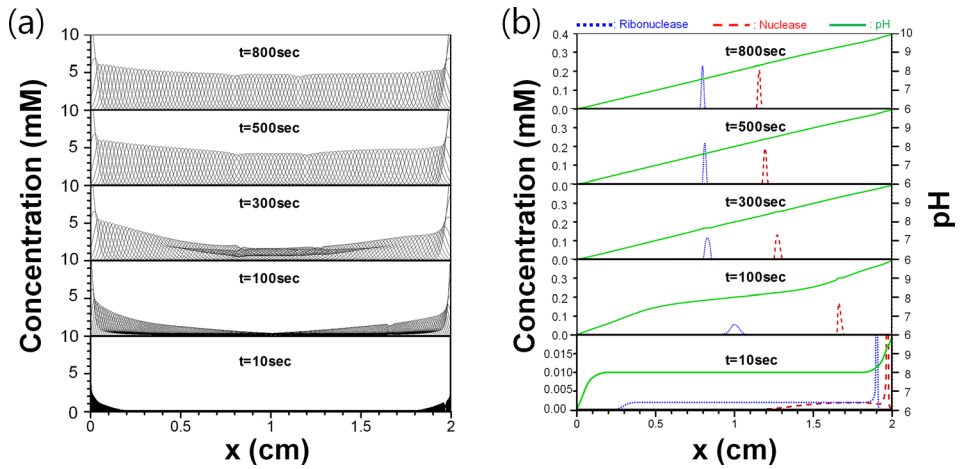


FIG. 5. Concentration distribution of (a) ampholytes and (b) proteins along a straight microchannel considering the Joule heating effect in microchip IEF. Temperature-dependent thermo-physical and electrochemical properties are used to take care of the temperature change in the channel during IEF. All other simulation conditions are the same as those shown in Fig. 4.

Second, the location of the focused protein bands moves toward the anolyte reservoir for temperature-dependent IEF. This occurs because the titration curve of the proteins is a strong function of temperature. As shown in Fig. 2, the isoelectric point of both proteins moves toward the left as the temperature changes from 25 to 100 °C. A comparison of focused protein locations between the Joule heating and no Joule heating cases is shown in Fig. 6 for identical IEF operating conditions. Due to Joule heating, the isoelectric point of nuclease shifts from 9.385 to 8.345, while the pI point of ribonuclease moves from 8.315 to 7.595 at 800 s. Since the focus positions of proteins are significantly different in temperature-dependent IEF, we must take this fact into consideration in microchip design and further analysis of proteins. For instance, proteins are generally mobilized to a detector point at the end of the separation, and the mobilization scheme is based on the final focused position of the proteins. If the location of focused proteins is not identified properly, the experiment design for further analysis will be faulty. Figure 6 also shows a peak concentration comparison between the Joule heating and no Joule heating cases. At the fully separated stage, the peak concentrations of proteins are almost identical for the Joule heating and no Joule heating cases. However, noticeable differences in the transient concentration distribution are observed between the Joule heating and no Joule heating cases, especially for ribonuclease.

Furthermore, the separation resolution is highly affected by Joule heating in the system. Figure 7 shows separation performance with and without Joule heating effect in an ampholyte based microchip IEF. As mentioned earlier, in temperature dependent IEF, the peak locations of both proteins shift towards the anodic side. At the end of the separation, the distance between two peaks decreases in Joule heating case compared to the no Joule heating case as shown in Figure 7(a). As the protein bands come closer, the resolution goes down in Joule heating case (Figure 7(b)).

To understand the effect of Joule heating in the separation process, the heat generation term due to the applied electric field must be determined. The heat generation term depends on the ionic conductivity and the local electric field in the channel. The ionic conductivity can be obtained from the concentration and net charge of all ionic components such as proteins, ampholytes, hydronium ions, and hydroxyl ions. Unlike linear electrophoresis (e.g., zone electrophoresis), the charge of all amphoteric components is a function of location. The net charge of proteins is calculated from titration curves, and the net charge of ampholytes is computed from Eq. (5) in order to calculate the ionic conductivity.

Figure 8 shows the ionic conductivity, electric field, and source term distribution along the channel for temperature-dependent IEF. Initially, the ionic conductivity (Fig. 8(a)) is very high

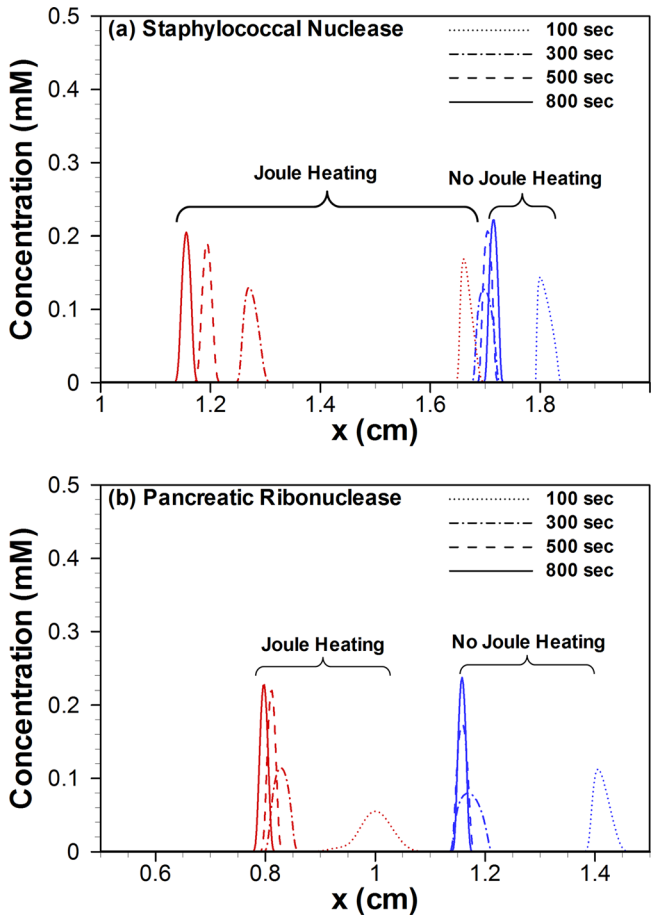


FIG. 6. Comparison of concentration profiles of proteins with and without Joule heating during IEF process in a straight microchannel for a nominal electric field of 100 V/cm.

throughout the channel because both proteins and the ampholytes are trying to focus at the isoelectric point. As time progresses, the ampholytes close to two electrode reservoirs focus first, and the focusing front moves toward the center of the channel (Fig. 5(a)). For that reason, the ionic conductivity is lower at two sides, but higher at the channel center at $t = 100$ s. The local peaks in the conductivity profile are primarily due to the high charges of proteins compared to the ampholytes in the system. Later in the separation process ($t > 300$ s), the ionic conductivity drops significantly throughout the channel, except at the locations of proteins, because of the

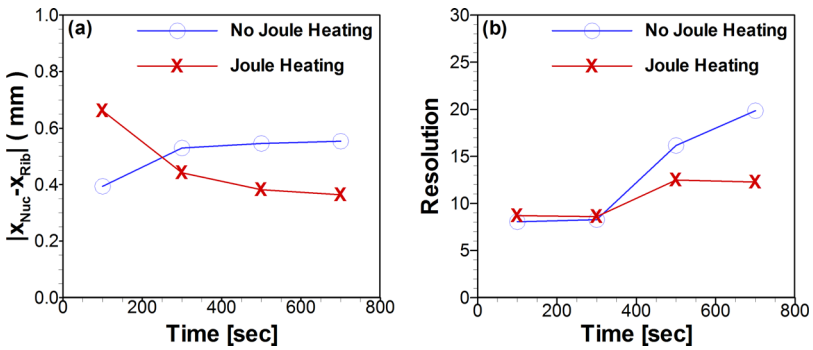


FIG. 7. Separation efficacy in microchip IEF with and without Joule heating: (a) Distance between two protein peaks and (b) separation resolution.

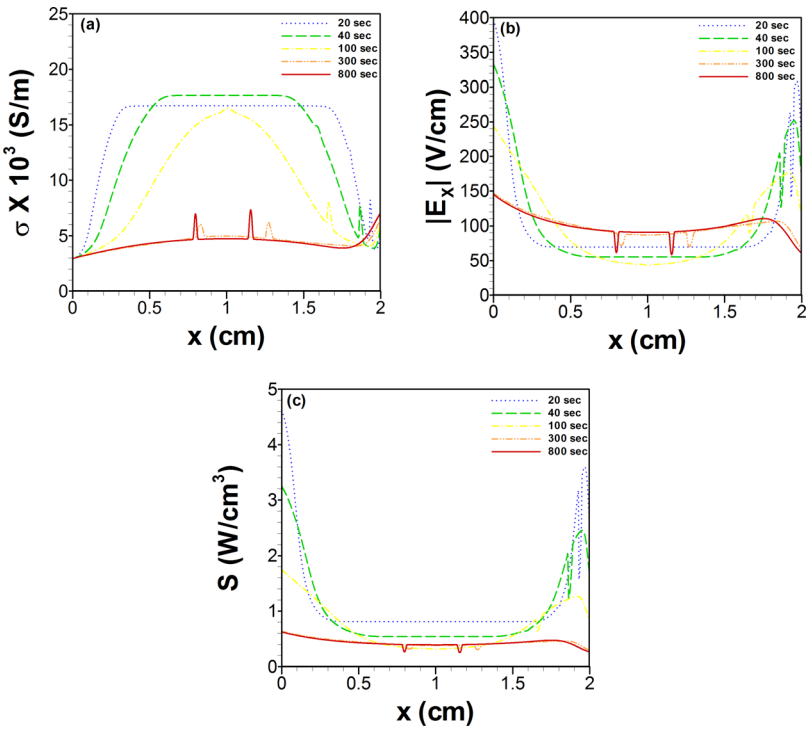


FIG. 8. (a) Conductivity, (b) electric field, and (c) heat generation distribution along the channel during IEF simulation. The potentials at the anodic and cathodic sides are 200 and 0 V, respectively. All other simulation conditions are the same as those shown in Fig. 5.

fact that most ampholytes have already reached their isoelectric points. It is interesting to note that the ionic conductivity increases sharply close to the cathode reservoir. This is due to the electroneutrality condition at the cathodic end. Due to the high pH at the cathodic end, the concentration of hydroxyl ions is much higher. The negatively charged hydroxyl ions should be balanced by the ampholytes, which causes localized stacking of ampholytes on the right side of the channel, resulting in higher ionic conductivity.

The electric field distribution is guided by the ionic conductivity as shown in Fig. 8(b). Thus, the local electric field will be lower at the region of higher ionic conductivity and vice versa. The trend for the source (Joule heat) term is very similar to the applied electric field since it is directly related to the second power of the local electric field. At the end of the separation process, the electric field-driven generation term is almost uniform throughout the channel (Fig. 8(c)).

### C. Temperature distribution due to Joule heating

To obtain the temperature distribution in the microchannel, the energy equation is solved with the source term due to Joule heating. In this study, constant temperatures are maintained at two reservoirs and insulating boundary conditions at all other boundaries. The constant temperature on the left and right boundaries can be justified because the size of the reservoirs is generally much larger than the microchannel, and there is no net mass transfer between the reservoir and microchannel due to advection, diffusion, or electro-migration. On the other hand, the insulating boundary conditions are appropriate for other boundaries since microchannels are generally made of glass, PDMS, or acrylic, which are thermally insulating. The simulation is carried out for an initial uniform temperature of 20 °C throughout the channel, and the temperatures of the anolyte and catholyte reservoir are set to 20 °C.

The transient temperature distribution along the channel is shown in Fig. 9(a) for temperature-dependent IEF with an applied potential difference of 200 V. At the early stage of

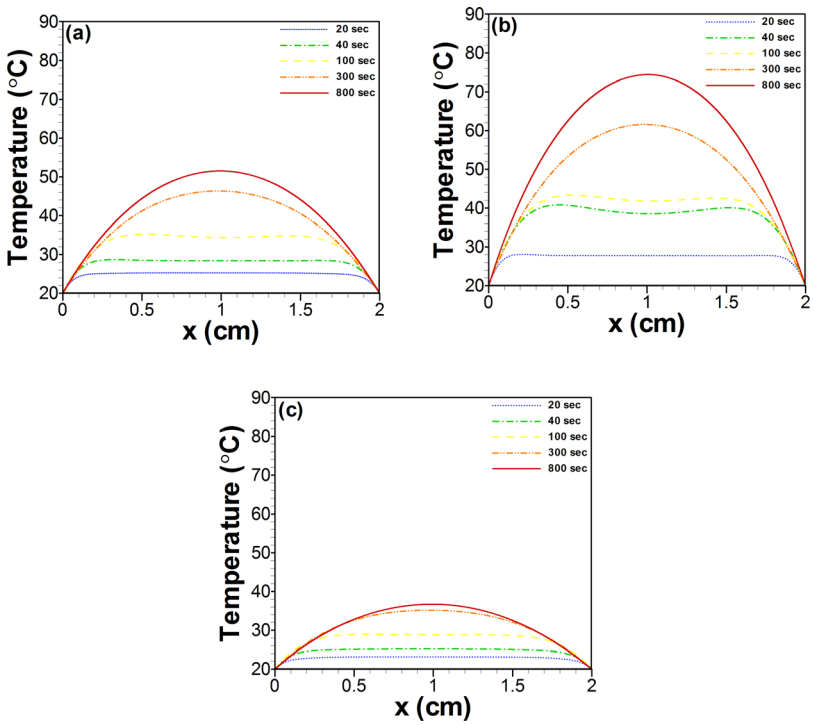


FIG. 9. Temperature distributions along the channel during the IEF process for a nominal electric field of (a) 100 V/cm, (b) 125 V/cm, and (c) 75 V/cm. All other simulation conditions are the same as those shown in Fig. 5. The end of the separation time is 1000 s, 800 s, and 500 s for a nominal electric field of 75 V/cm, 100 V/cm, and 125 V/cm.

separation, the temperature profile remains flat where the heat generation term is minimum and drops to the reservoir temperature at two sides to satisfy the imposed Dirichlet boundary conditions. Over time, the temperature along the channel goes up, primarily due to electric field-driven heat generation. Even though the magnitude of the heat generation term decreases with time (Fig. 8(c)), the temperature continues to increase because of the lack of an active cooling mechanism in the microchip IEF. Also, we note that unlike ITP, in IEF there is no net flow through the channel for the removal of heat. Thus, it is important to understand the hot spot in an IEF chip and identify the appropriate operating conditions such as an applied potential difference, separation time, etc. At 100 s, the dip in the temperature profile at the middle of the channel is due to a decrease in the generation term, primarily in the mid-section of the channel. At the end of the separation phase, the temperature distribution is parabolic in shape due to almost uniform heat generation in the channel. This scenario is similar to the temperature distribution in a nonmoving fluid or solid with uniform generation, except that the temperature profile is not symmetric (Fig. 9). The slightly skewed temperature profile is due to complex heat generation distribution in the channel, which changes with time as shown in Fig. 8(c).

In microchip IEF, the temperature rise worsens at a higher applied electric field, as shown in Fig. 9(b). In this case, the applied potential difference between anode and cathode reservoirs is 250 V. Although the fluid temperature increases at a much higher rate, the overall trends in temperature profiles remain the same, as in the case shown in Fig. 9(a). It is important to note that a higher applied electric field also shortens the separation time considerably. In other words, ampholytes and proteins start moving toward their isoelectric point quickly, resulting in smaller ionic conductivity in the middle section of the channel. This fact contributed to a dip in temperature at the channel center at 40 s. For a low applied potential difference, the temperature rise is quite moderate, as shown in Fig. 9(c). However, in this case, the separation is not complete at 800 s. In fact, it requires 1000 s to complete the separation. The maximum temperature at the end of the separation is 37 °C, which is still reasonably small in terms of affecting the final location of the separated bands. These numerical results indicate that applied nominal

electric field should not be higher than 125 V/cm for microchip IEF to avoid thermal denaturation of proteins as well as evaporation of carrier electrolyte.

### D. Effect of ampholyte dissociation constants on maximum temperature

Next, we studied the effect of the dissociation constants of ampholytes for the effective separation of proteins. In this study, we considered biprotic ampholytes for simplicity in our calculations. Biprotic ampholytes can have three charge states ($z = -1$, 0, and 1) and two dissociation constants ($K_1$ and $K_2$). Previous numerical results have shown that the separation results significantly depend on the selection of dissociation constants or $\Delta pK = -\log_{10}(K_2/K_1)$.[34]

IEF separation can be completed quickly with ampholytes having a smaller value of ΔpK. For instance, separation can be completed in less than 90 s if $\Delta pK = 0.2$, while it takes more than 10 min for ΔpK greater than 2. Although a smaller value of ΔpK is preferred for quick IEF separation because the temperature increase will be negligible in the first 2 min, in reality it is not practical to have biprotic ampholytes with a ΔpK value of less than 2. Thus, we have studied the thermal characteristics in microchannel IEF for different values of ΔpK ranging from 2.25 to 3. Figure 10 shows the maximum temperature in a 2 cm-long IEF channel for a nominal electric field of 100 V/cm. As previously mentioned, the separation can be completed faster for a smaller value of ΔpK. For example, the end of the separation time is 260, 340, 500, and 700 s for ΔpK of 2.25, 2.5, 2.75, and 3.0, respectively, and thus the maximum temperature distribution (Fig. 10) is presented for different time durations. Numerical results reveal that the maximum temperature decreases with increasing ΔpK. This is because of the lower heat generation term at a higher ΔpK value, as shown in Fig. 11(a). It is noteworthy to mention that the source terms for different ΔpK values are obtained at the end of the separation stage. As the ΔpK of ampholytes increases, the ionic conductivity decreases since the net charge distribution of ampholytes takes place over a wider pH range. This means that the contribution of charges diminishes quickly outside the isoelectric points of the ampholytes, resulting in low ionic conductivity at a high ΔpK value, as shown in Fig. 11(b).

### E. Effect of Joule heat in pH supplied/actuated microchip IEF

Recently, Cheng and Chang[4] have developed a microfluidic based IEF platform in which the pH profile is formed by supplying hydrogen and hydroxyl ions in the separation channel. In their study, hydrogen and hydroxyl ions are produced by a field induced water dissociation

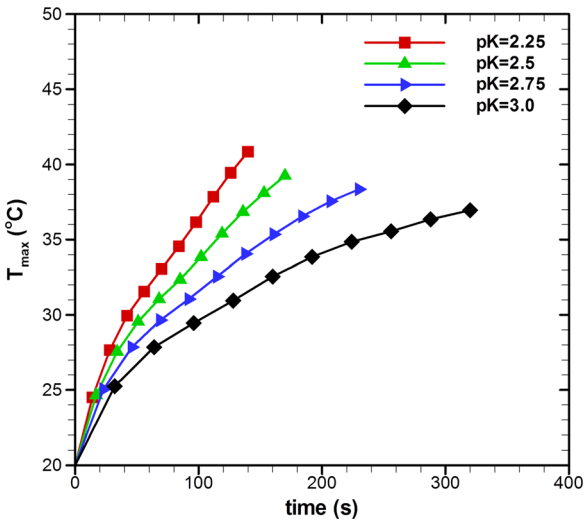


FIG. 10. Maximum temperature in an IEF microchannel for different values of ΔpK. Results are shown for different times since the end of the separation time changes with ΔpK. The potentials at the anodic and cathodic side are 200 and 0 V, respectively. All other simulation conditions are the same as those shown in Fig. 5.

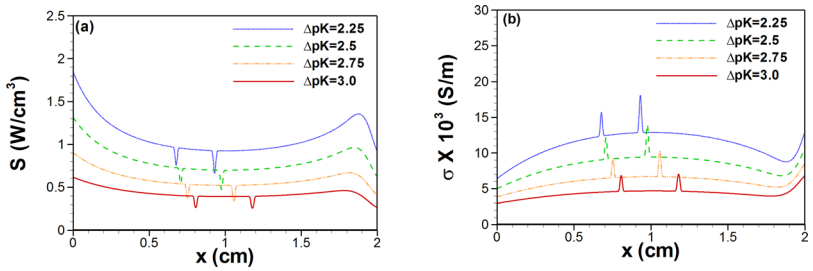


FIG. 11. (a) Heat generation and (b) conductivity distribution along the channel during IEF simulation for different values of ΔpK. The nominal electric field is 100 V/cm. Results are presented at the end of separation. The approximate end of the separation times are 300, 400, 500, and 600 s for ΔpK = 2.25, 2.5, 2.75, and 3.0 respectively.

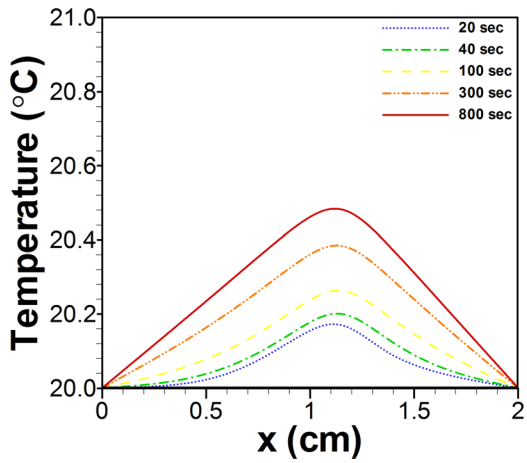


FIG. 12. Temperature distribution along the channel during sample separation in pH actuated IEF for a nominal electric field of 125 V/cm. Here, pH profile is assumed linear along the channel as shown in Ref. 4, and mass conservation equations are not solved for ampholytes. All other simulation conditions are the same as those shown in ampholyte based IEF.

phenomenon.[19] This new separation platform is capable of creating pH without supplying ampholytes in the system. To understand the heat generation in their microfluidic separation system and compare that with the traditional microchip IEF, we have simulated the IEF separation for their system. For the sake of comparison with our ampholyte based IEF system, we have considered only IEF in a straight channel (2 cm × 100 $\mu$m × 10 $\mu$m) considering a pH range of 2 to 11, and two sample proteins (staphylococcal nuclease and pancreatic ribonuclease) are allowed to separate at a nominal electric field of 125 V/cm. Figure 12 shows the transient temperature rise predicted by our model for a microchip IEF where pH is created by supplying ions. Unlike ampholyte based IEF, the temperature rise is very minimal when pH is created by supplying hydrogen and hydroxyl ions. This is due to the fact that ionic conductivity of the buffer solution is very low for this case. In ampholyte based IEF, conductivity is very high at the initial separation phase as ampholytes try to focus at their pI points. This high conductivity is responsible for large Joule heat, which can be avoided in the new microfluidic format proposed in Ref. 4. Furthermore, the Joule heat could be removed from the system if a flow field is introduced perpendicular to the applied electric field.[12] However, further study is needed to quantify fluid flow strength to overcome Joule heating problem, while maintaining a very good separation.

## VI. CONCLUSIONS

A mathematical model is presented for temperature-dependent IEF. The model was used to study the effect of Joule heating on protein separation behavior. Unlike constant temperature

IEF, the effect of temperature change in the IEF process is accounted for by temperature-dependent thermo-physical properties such as density, specific heat, thermal conductivity, ionic conductivity, and diffusion coefficient, and by electrochemical properties such as absolute mobility and temperature-dependent net charge. A finite volume-based numerical model is presented to solve coupled mass, charge, and energy conservation equations for temperature-dependent IEF. Numerical results for temperature-dependent IEF are obtained for the transient separation of two model proteins (staphylococcal nuclease and pancreatic ribonuclease) in a pH range from 6 to 10 using 100 biprotic ampholytes. The simulation results are compared with constant temperature IEF in which the contribution of the electric field-driven Joule heating term is ignored. It was found that the focusing of ampholytes gets faster for the Joule heating case compared to the no Joule heating case. Joule heating has a significant effect on the final location of focused proteins because the isoelectric point is a strong function of temperature. This finding is in line with the experimental observation in microchip IEF.[3] Identification of the final focus point of the proteins is very important for optimum protocol design in microchip IEF. Numerical results also show that the Joule heating effect worsens at a higher electric field. Thus, attention should be given in selecting the applied electric field for microchip IEF by considering the separation time and maximum temperature in the separation channel. We also studied the effect of ampholyte dissociation constants on temperature-dependent IEF. As expected, the separation time decreases as the ΔpK of the ampholytes decreases. However, the maximum temperature rise in the channel increases with a decrease in ΔpK of the ampholytes. That is, the detrimental effect is worse for low ΔpK values of ampholytes, even though protein separation can be achieved quickly. Numerical results also show that the detrimental effect of Joule heat is negligible in microchip IEF when pH is formed by supplying hydrogen and hydroxyl ions instead of ampholytes.

## ACKNOWLEDGMENTS

This work was supported by Yeungnam University research grants in 2013.

## APPENDIX A: JOULE HEATING CONTRIBUTION TO AN ELECTROSEPARATION PROCESS

Derivation of Joule heating term for microchip IEF: In an electrolyte, the local heat generation due to applied electric current can be expressed as

$$q = \vec{I} \cdot \vec{E}, \tag{A1}$$

where $q$, $\vec{I}$, and $\vec{E}$ are the heat generation per unit volume, current density vector, and electric field strength, respectively. In an electrokinetic process, the current density vector can be described as

$$\vec{I} = F \sum_i \left[ \sum_j z_{ij} S_{ij} \vec{V}_{ij} \right], \tag{A2}$$

where F is the Faraday constant, and $z_{ij}$, $S_{ij}$, and $\vec{V}_{ij}$ are the charge number, concentration, and total velocity of the species, respectively. The total velocity of each species consists of electro-migration ($\vec{V}_{ij_e}$), diffusion ($\vec{V}_{ij_d}$), and bulk fluid ($\vec{V}_{bulk}$) velocity as follows:

$$\vec{V}_{ij} = \vec{V}_{ij_e} + \vec{V}_{ij_d} + \vec{V}_{bulk}. \tag{A3}$$

The diffusion and electro-migration velocity of each species can be obtained from Fick's law and the electro-migration force as follows:

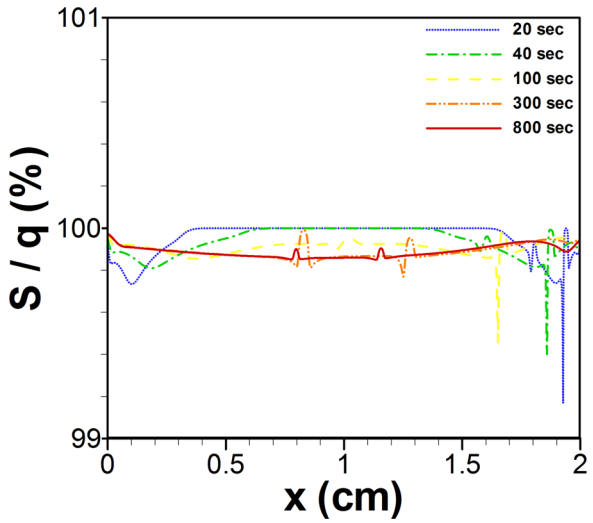


FIG. 13. Joule heat (source) term distribution along the channel at different times. The contribution of the diffusion term is less than 1% in microchip IEF.

$$\vec{V}_{ij\,d} = -D_{ij}\frac{\nabla S_{ij}}{S_{ij}} \tag{A4a}$$

$$\vec{V}_{ij\,e} = z_{ij}\omega_{ij}\vec{E}, \tag{A4b}$$

where $D_{ij}$ and $\omega_{ij}$ are the diffusion coefficient and absolute mobility of the species. By substituting Eqs. (A3) and (A4) into Eq. (A2), we obtain the following expression for the current density vector:

$$\vec{I} = \vec{E}F\sum_i\left[\sum_j(z_{ij}{}^2\omega_{ij}S_{ij})\right] - F\sum_i\left[\sum_j(z_{ij}D_{ij}\nabla S_{ij})\right] + F\sum_i\left[\sum_j(z_{ij}S_{ij}\vec{V}_{bulk})\right]. \tag{A5}$$

By using the relationship between species and the components for mass (Eq. (3)) and charges (Eqs. (5) and (7)), and by assuming uniform absolute mobility ($\omega_{ij} = \omega_i$) and uniform diffusion coefficient ($D_{ij} = D_i$) for each species of component (i), the current density can be rewritten as

$$\vec{I} = \vec{E}F\sum_i(\langle z_i{}^2\rangle\omega_i C_i) - F\sum_i(\langle z_i\rangle D_i\nabla C_i) + F\sum_i(\langle z_i\rangle C_i\vec{V}_{bulk}). \tag{A6}$$

By substituting Eq. (A6) into Eq. (A1), the Joule heat term can be obtained as

$$q = \sigma\vec{E}\cdot\vec{E} - F\sum_i(\langle z_i\rangle D_i\nabla C_i\cdot\vec{E}) + F\sum_i(\langle z_i\rangle C_i\vec{V}_{bulk}\cdot\vec{E}), \tag{A7}$$

where $\sigma$ is the ionic conductivity of the electrolyte defined in Eq. (2). The first term of the aforementioned equation is same as in a solid electrolyte; the second and third terms appear due to ion transport in an electrolyte. In an IEF system, no external flow is applied to reduce the dispersion of separated bands. Thus, the contribution of the third term is negligible in the Joule heating equation. The contribution of the second term is important where there is a high concentration gradient. However, in an IEF system, the net charge is very small at the location of a high concentration gradient. So, the contribution of the second term is also negligible, as shown in Fig. 13.

[1]H. C. Cui, K. Horiuchi, P. Dutta, and C. F. Ivory, Anal. Chem. **77**(24), 7878–7886 (2005).
[2]A. E. Herr, J. I. Molho, K. A. Drouvalakis, J. C. Mikkelsen, P. J. Utz, J. G. Santiago, and T. W. Kenny, Anal. Chem. **75**(5), 1180–1187 (2003).

[3]H. C. Cui, K. Horiuchi, P. Dutta, and C. F. Ivory, Anal. Chem. **77**(5), 1303–1309 (2005).
[4]L. J. Cheng and H. C. Chang, Lab Chip **14**(5), 979–987 (2014).
[5]M. Bier, O. A. Palusinski, R. A. Mosher, and D. A. Saville, Science **219**(4590), 1281–1287 (1983).
[6]J. Shim, P. Dutta, and C. F. Ivory, J. Mech. Sci. Technol. **23**(12), 3169–3178 (2009).
[7]K. Yoo, J. Shim, J. Liu, and P. Dutta, Electrophoresis **35**(5), 638–645 (2014).
[8]R. A. Mosher and W. Thormann, Electrophoresis **23**(12), 1803–1814 (2002).
[9]R. A. Mosher and W. Thormann, Electrophoresis **29**(5), 1036–1047 (2008).
[10]J. Shim, P. Dutta, and C. F. Ivory, Electrophoresis **30**(5), 723–731 (2009).
[11]J. Shim, P. Dutta, and C. F. Ivory, Electrophoresis **28**(4), 572–586 (2007).
[12]K. Yoo, J. Shim, J. Liu, and P. Dutta, Biomicrofluidics **8**(3), 034111 (2014).
[13]B. Kates and C. L. Ren, Electrophoresis **27**(10), 1967–1976 (2006).
[14]P. Dutta, K. Horiuchi, and H. M. Yin, Comput. Math. Appl. **52**(5), 651–670 (2006).
[15]K. Horiuchi, P. Dutta, and A. Hossain, J. Eng. Math. **54**(2), 159–180 (2006).
[16]E. Grushka, R. M. McCormick, and J. J. Kirkland, Anal. Chem. **61**(3), 241–246 (1989).
[17]S. Ghosal, *Annual Review of Fluid Mechanics* (Annual Reviews, Palo Alto, 2006), Vol. 38, pp. 309–338.
[18]J. Shim and P. Dutta, Int. J. Nonlin. Sci. Numer. Simul. **13**(5), 333–344 (2012).
[19]L. J. Cheng and H. C. Chang, Biomicrofluidics **5**(4), 046502 (2011).
[20]K. Horiuchi and P. Dutta, Int. J. Heat Mass Transfer **47**(14–16), 3085–3095 (2004).
[21]D. A. Saville and O. A. Palusinski, AIChE J. **32**(2), 207–214 (1986).
[22]R. A. Mosher, D. A. Saville, and W. Thormann, *The Dynamics of Electrophoresis* (VCH, Weinheim, 1992).
[23]T. Z. Jubery, A. S. Prabhu, M. J. Kim, and P. Dutta, Electrophoresis **33**(2), 325–333 (2012).
[24]J. Lindner, D. Snita, and M. Marek, Phys. Chem. Chem. Phys. **4**(8), 1348–1354 (2002).
[25]M. Pribyl, D. Snita, and M. Marek, Chem. Eng. J. **105**(3), 99–109 (2005).
[26]S. Ghosal, J. Fluid Mech. **459**, 103–128 (2002).
[27]S. Ghosal, J. Fluid Mech. **491**, 285–300 (2003).
[28]W. Thormann, J. Caslavska, and R. A. Mosher, J. Chromatogr. A **1155**(2), 154–163 (2007).
[29]R. C. Weast, *CRC Handbook of Chemistry and Physics* (CRC Press, Boca Raton, FL, 1988).
[30]G. Tang and C. Yang, Electrophoresis **29**(5), 1006–1012 (2008).
[31]H. Nagai, K. Kuwabara, and G. Carta, J. Chem. Eng. Data **53**(3), 619–627 (2008).
[32]J. M. Dick, D. E. LaRowe, and H. C. Helgeson, Biogeosciences **3**(3), 311–336 (2006).
[33]S. V. Patankar, *Numerical Heat Transfer and Fluid Flow* (Taylor and Francis, USA, 1980).
[34]J. Shim, P. Dutta, and C. F. Ivory, J. Nanosci. Nanotechnol. **8**(7), 3719–3728 (2008).